Applied Ocean Research 166 (2026) 104905

Contents lists available at ScienceDirect

Applied Ocean Research

journal homepage: www.elsevier.com/locate/apor

Research paper

Physical modelling of the SeAbacus wave energy converter

Barbara Zanuttigh *, Paola Pareschi, Elisa Dallavalle, Sara Mizar Formentin, Maria Gabriella Gaeta

Department of Civil, Chemicals, Environmental and Material Engineering, University of Bologna, Viale Risorgimento 2, Bologna 40136, Italy

ARTICLE INFO

Keywords:
Wave energy
Wave attenuator
Salter's duck
Wave tank
Moorings
Pitch

ABSTRACT

The SeAbacus is a new patent for a floating offshore wave attenuator, which essentially consists of a rafted Salter's Duck. It is modular, suitable also for low-energy seas and for array installation. This paper presents the first physical model tests carried out in the wave tank at the Hydraulic Laboratory of the University of Bologna. The tests focused on the effects of the device shape (by changing the shape of the Salter's Duck) and of the mooring layout (by testing a Tension Leg Platform, a Catenary Anchor Leg Mooring configuration and a spread mooring system) under wave attacks characterised by different wave height, wave steepness and wave obliquity. The results of the tests highlight the relevance of the shape of the Salter's Duck and the capability of the device of producing wave energy also in mild seas, provided a moderate wave steepness. Wave obliquity significantly decreases the device pitch motion. The mooring layout affects the device motions because the more rigid the moorings the higher the device pitch due to combined motions of the raft and of the Salter's Duck. The best compromise between device pitch motions and mooring loads was achieved with the spread mooring system.

1. Introduction

Wave Energy Converters (WECs) have been the subject of extensive and ongoing patent activity, with a remarkable number of patents filed from the 1970s to the present (Falcão, 2010; Koca et al., 2013; Guo and Ringwood, 2021; Bouhrin et al., 2024). The patents encompass a wide variety of WECs, which differ significantly in terms of operating principles and installation methods. However, to date, no technology has established itself over the others and very few devices have reached commercialization (Foteinis and Tsoutos, 2017; Aderinto and Li, 2018). There are still technological and non-technological barriers to be overcome and some of these are specifically related to the new device that will be the subject of this paper.

As widely documented in the literature, mooring systems often represent the most significant cost component for WECs, due to the complexity of their design and to the challenges associated with offshore installation. Recent reviews on mooring lines materials, mooring configurations, modelling and design were provided by Xu et al. (2019), Qiao et al. (2020), Chatzigiannakou and Temiz (2021). The importance of mooring system design for WEC producibility was also highlighted by Zanuttigh et al. (2013), Martinelli et al. (2018), Niosi et al. (2021) and Zhao et al. (2025).

Another major cost driver for WECs lies in the complexity of their structures, which typically require custom design and dedicated manufacturing processes, see Guo and Ringwood (2021), Golbaz et al. (2022), and Garcia-Teruel and Forehand (2021). Golbaz et al. (2022) concluded that shape optimization can significantly improve performance and reduce costs, especially when combined with an appropriate Power Take-Off (PTO) control strategy. However, Garcia-Teruel and Forehand (2021) observed that most shape optimization studies have neglected manufacturability, a critical factor in assessing whether the optimized geometry will actually result in lower Levelized Cost of Energy (LCOE).

Materials play a crucial role in the sustainability of WEC installations. Bruno et al. (2022) demonstrated that the main environmental impacts come from manufacturing processes and from the limited durability of materials. Calvario et al. (2017) and Arredondo-Galeana et al. (2023) showed that composite materials can offer advantages in terms of durability, ease of manufacturing and maintenance with respect to steel. The relevance of steel reduction in minimizing the carbon footprint was also emphasized by Jahangir et al. (2025).

This paper presents a new Italian patent, the SeAbacus (patent no. 102022000002747), a floating wave attenuator device currently at Technological Readiness Level (TRL) 4, and the tank tests of the device to evaluate its motions and potential producibility. The SeAbacus is meant for partially overcoming the aforementioned barriers. The device

* Corresponding author.
E-mail address: barbara.zanuttigh@unibo.it (B. Zanuttigh).

https://doi.org/10.1016/j.apor.2025.104905
Received 3 August 2025; Received in revised form 14 December 2025; Accepted 24 December 2025
Available online 15 January 2026

components can be easily manufactured or are already commercially available, the device does not include exposed components to avoid debris in the sea, the device materials for future construction at prototype scale are polymers and composites to contemporarily improve the power production by reducing the device inertia and significantly reduce the environmental impact of the steel-equivalent device.

The SeAbacus is essentially a rafted oscillating element whose shape is similar to a Salter's Duck (Salter, 1974). It is not the first attempt to modify the original Salter's Duck wave energy converter, there are other options in the literature, a.o. the solo Duck, which is able to use the point absorber effect to further enhance its power capture performance (Wu et al., 2017); a solo circular cylinder for desalination purpose with an offset pitching axis without the front beak to replace the original shape and reduce cost (Cruz et al., 2006); a modified Duck that adopts a new type of underwater-stabilized substrate (Zhang et al., 2019); the WEPTOS device, which has two symmetrical linear arrays arranged in an A-shape configuration (Margheritini and Kofoed, 2019). Recently, Yazdi et al. (2023) proposed the integration of an array of Salter's Duck with a floating off-shore wind turbine.

Compared to existing devices, the innovative nature of SeAbacus consists in the simultaneous achievement of the following objectives: i) it has a modular shape that facilitates its installation in parks; ii) it has low inertia to generate energy even in mild climate seas; iii) it does not contain mechanical parts exposed to waves, to avoid the formation of debris in the sea; iv) its dimensions are scalable depending on the climate and it can be installed both in shallow waters, where maintenance is simpler and anchoring is less expensive, and in deep waters, where the harvestable wave energy is greater; v) it is easy to build and maintain, as it has a simple geometry, made up of industrially available parts, to minimize production times and costs, and it is easily disassembled, to minimize maintenance costs; vi) it is assumed to adopt a proven electromagnetic energy conversion system, developed by the IMAGINE project (Imagine, 2020), capable of producing energy in both directions of rotation; vii) it is low in the water and buoyant, therefore it has little visual and environmental impact, to increase social acceptance.

The paper structure is as follows. Section 2 presents the experimental set-up, including the facility, the device, the mooring layouts, the measurements and the tests. Section 3 describes the results in terms of the effects of the device shape, of the mooring system and of the wave obliquity on the device motions (i.e. specifically the pitch) and therefore on its potential producibility. Section 4 details the forces on the different mooring system and discusses the combined forces-potential producibility depending on the mooring layout. Conclusions are finally drawn in Section 5.

2. The experimental set-up

2.1. The wave basin

The tests were performed in the wave basin of the Hydraulic Engineering Laboratory of the University of Bologna, which was built thanks to regional POR-FESR funds and ministerial funds for Excellent Departments. The tank has dimensions 17 × 10 × 1.4 m^3. It is equipped with 16 plunging modules controlled by vertical axis pistons (plunger wavemaker) that generate, thanks to calibrated transfer function in Awasys software by Aalborg University (2018), a multidirectional wave motion (± 20°), regular or irregular, with significant wave height and typical wave period in the range of 0.01-0.2 m and 0.5-2 s, respectively, with a water depth between 0.4 and 1 m. The tank is equipped with passive absorption, realized by means of boxes filled-in with honeycomb plastic material and placed along the side of the tank opposite to the wavemaker.

2.2. The device

The proposed device, called SeAbacus (Fig. 1) is a floating device,

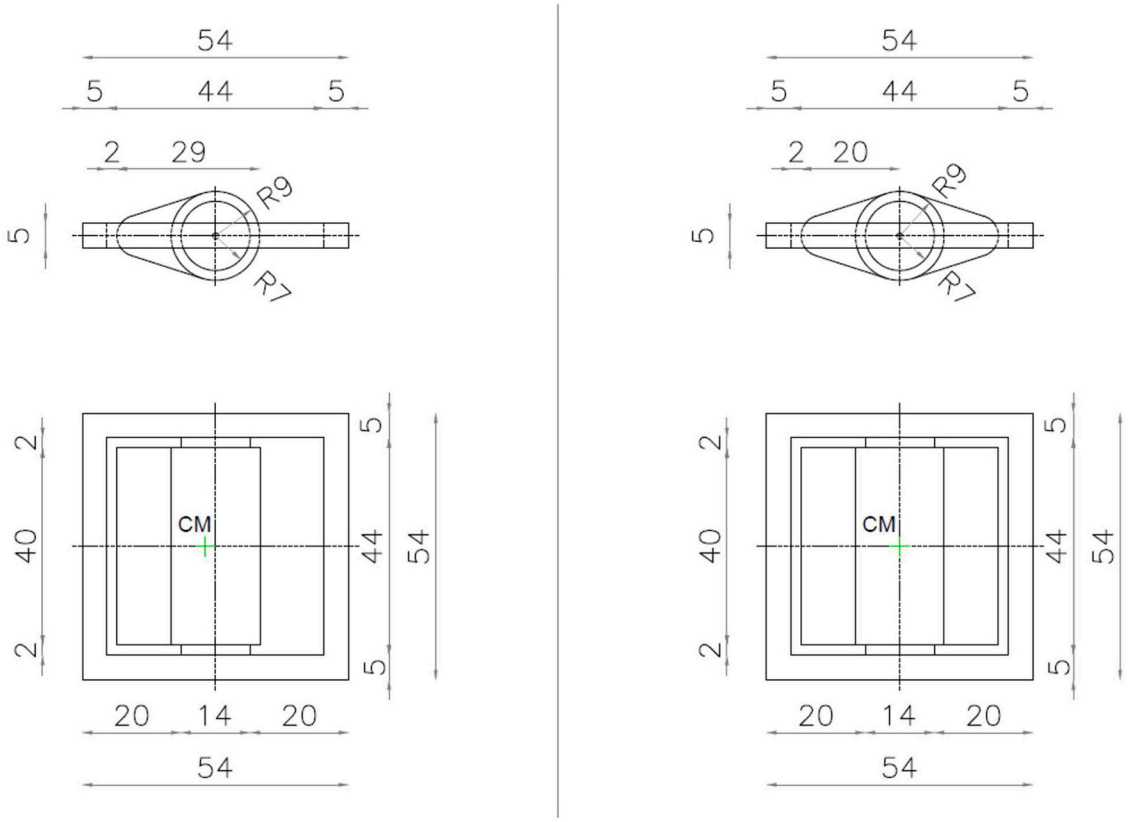

Fig. 1. Side scheme (top) and top view (bottom) of the SeAbacus with main dimensions. To the left, Single Salter's Duck (SD); to the right, Double Salter's Duck (DD).

small in size, barely emerging from the water, compact and devoid of fragile mechanical parts exposed to the waves. It consists of a raft, which stabilizes the device, and an oscillating element, whose shape is similar to a Salter's Duck (Salter, 1974). The oscillating element rises when the crest passes and lowers when the trough passes, possibly determining the rotation of the rotor of a reversible electromagnetic energy generation system, where the stator is fixed to the raft. The internal part of the oscillating element is therefore substantially different from the Salter's Duck, where the wave motion causes four gyroscopes inside to move back and forth, creating hydraulic energy that is transferred to a turbine or generator.

The SeAbacus (whose name comes from its shape similar to an abacus when placed in parks) for tank tests is made of aluminium. The raft is made of four square-section tubes that form a square ring with an external side of 0.54 m, and acts as a support for a rotating element (placed at the centre of the raft itself). In particular, two different shapes of the oscillating element were considered (Figs. 1 and 2): one of the "Single Salter's Duck" (SD) type and the other of the "Double Salter's Duck" (DD) type. The PTO system was not installed on the device therefore the potential producibility was indirectly assessed by measuring the pitch of the oscillating element through a Xsens inertial sensor. The moment of inertia of the DD and SD configurations with respect to the rotation axis of the oscillating element are respectively 0.074 and 0.063 kgm^2. The position of the mass centre (CM) for each configuration is reported in Fig. 1 with respect to the axes with origin in the device centre (for DD, CM has coordinates 0, 0, 0 while for SD, CM has coordinates 0, 2.08, 0 cm).

2.3. The mooring layouts

Given the non-negligible effects of mooring systems on the device producibility (Zanuttigh et al, 2013; Cerveira et al., 2013; Martinelli et al, 2018; Xu et al, 2021), three different moorings were tested: a Tension Leg Platform system (TLP), a Catenary Anchor Leg Mooring configuration (CALM) and a spread mooring system (SPREAD). Fig. 3 shows the mooring plan-layout for both CALM and spread configurations, while Fig. 4 shows the cross-shore sections for all the three types. In all the layouts the four mooring lines were made with 0.90 mm diameter nylon thread (0.75 g/m mass per unit length, 35 kg breaking load), iron carabiners and iron tie rods to adjust the length of the cable. In all the layouts, the WEC or the buoy were anchored to the seabed with the mooring lines and fo-ur 5 kg dead-weights, characterized by cylindrical shape (diameter 0.2 m, thickness 0.02 m) and made of steel. In the CALM system, the buoy was connected to the device by a synthetic rope that is of the same type used to connect the back of the WEC to the dead weight placed on the seabed. These synthetic ropes were slack and are placed only to avoid free drift of the WEC in the wave basin. The dead weight consisted of a 40 kg lead bar. It is worthy to note that there was no interference between the device and the buoy. The buoy moved "as a flap" without any contact with the device, keeping its position, to let the device able to move as free as possible.

2.4. The measurements

Surface water levels in the tank were measured using a group of 5 resistive probes in front of the wave maker at a distance of about one wave length from the floating device (Fig. 3). The placement of this number of wave gauges allowed to apply wave directional analysis and to evaluate the incident and reflected wave. Water levels were acquired with a frequency of 100 Hz. The load on the moorings was measured using 4 Futek submersible load cells with a full scale of 450 N and an acquisition frequency of 1 kHz. The rotation of the oscillating element was measured using 1 MTi-630 inertial sensor, characterized by an accuracy of 0.2° RMS on pitch and roll; the acquisition frequency was kept constant at 100 Hz.

2.5. The tests

Irregular waves with Jonswap spectrum were generated, perpendicular to the device placed at the center of the tank. The target significant wave height H_s varied between 0.02 and 0.08 m, the peak steepness for irregular waves, sop, varied between 0.010 and 0.025. The water depth h was kept constant h=0.70 m. The waves were almost all generated in intermediate conditions and did not give rise to breaking. A series of 500 waves was generated for each test, to be statistically representative also of complex wave-device interactions processes (Romano et al., 2014). The wave characteristics were selected to reproduce the mild climate of the Mediterranean Sea and specifically the most unfavourable wave conditions for energy production of the Northern Adriatic Sea, where Hs≤2 m for the 95% of the year and sop≤0.03 for the 59% of the year (Katalinić et al, 2018). The scale of the tests is therefore supposed to be 1:25 as for the representation of the wave climate.

A set of 13 irregular wave states was examined for both SD and DD configurations, see Table 1, in case of TLP mooring. These same 13 irregular wave states were reproduced also i) for the SD configuration with both spread and calm mooring system and ii) for the only case of the spread mooring, by changing the device obliquity with respect to the wave basin axis, obtaining two oblique configurations at 15° and 30°. Therefore, a total of 78 tests were carried out.

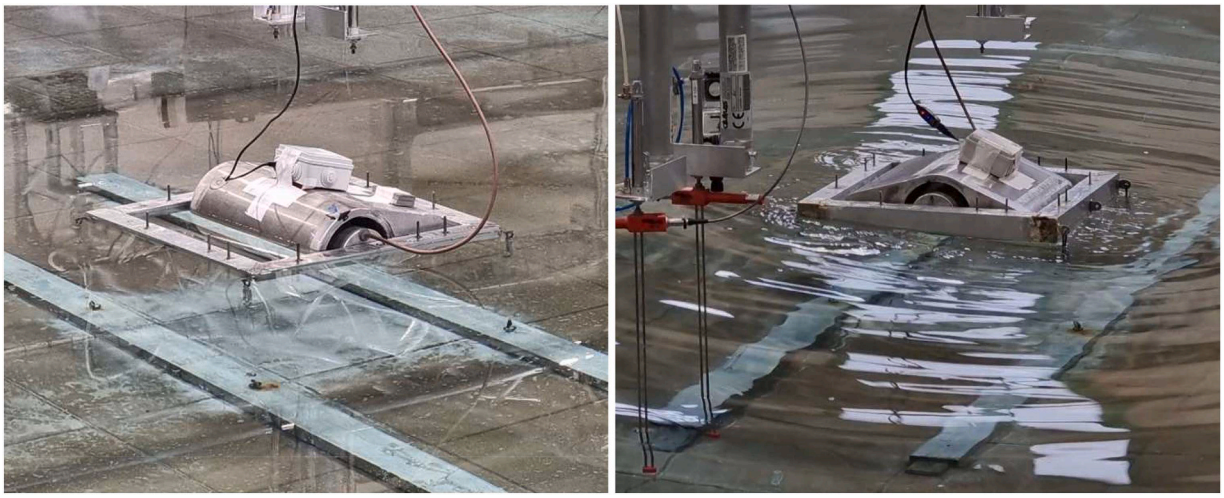

Fig. 2. Side view of the SeAbacus in the wave basin. To the left, Single Salter's Duck (SD); to the right, Double Salter's Duck (DD).

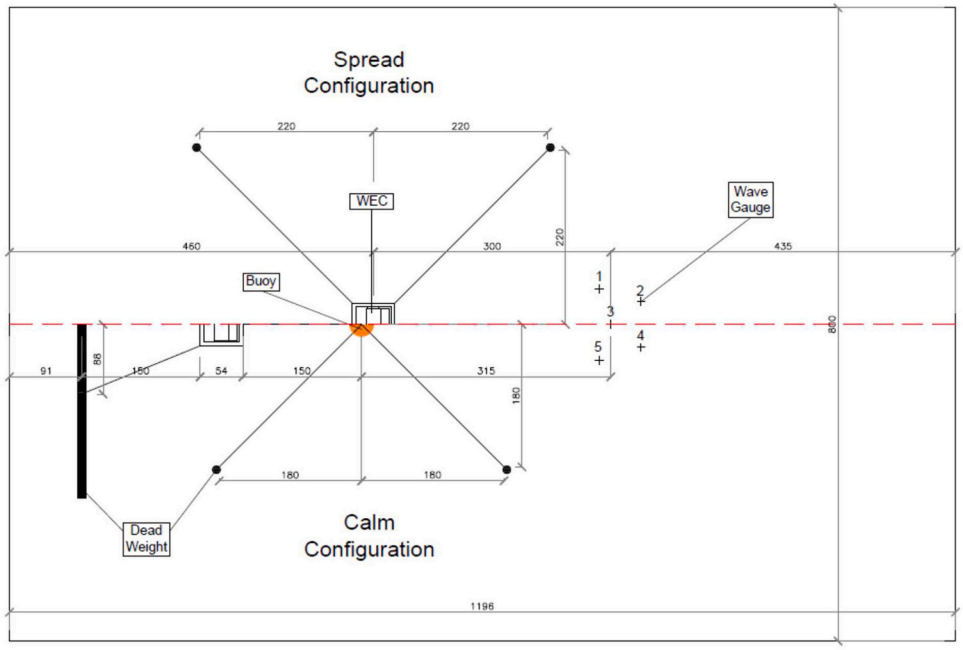

Fig. 3. Mooring layouts in the inner part of the wave basin. The side walls are made of steel plates, the offshore boundary (here to the right of the image) consists of the wave maker, the inshore boundary (here to the left) consists of absorbing caissons. The half basin above its cross-shore axis represents the case of the spread mooring, while the half basin below its cross-shore axis represents the case of the CALM mooring.

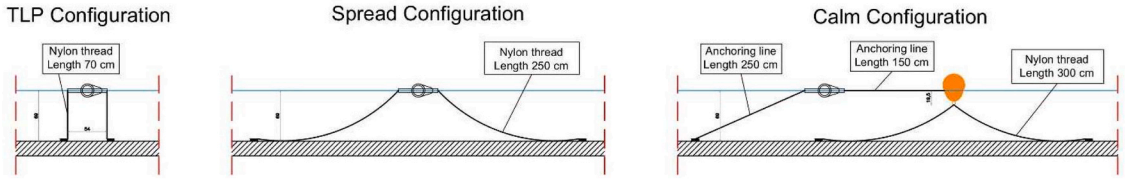

Fig. 4. Cross-shore sections of the three mooring types.

Table 1
Target values (H_s, Tp) and generated characteristics (Hsi, Ts) of the tested irregular (IR) wave attacks with different wave obliquities (β).

				β=0°		β=15°		β=30°	
IR	Hs, m	Tp, s	sop []	H_{si}, m	Ts, s	H_{si}, m	Ts, s	H_{si}, m	Ts, s
1	0.02	1.13	0.010	0.022	1.132	0.0195	1.063	0.020	1.062
2	0.02	0.80	0.020	0.021	0.800	0.020	0.771	0.020	0.770
3	0.03	1.13	0.010	0.034	1.132	0.029	1.060	0.029	1.06
4	0.03	0.98	0.020	0.034	0.980	0.030	0.923	0.030	0.925
5	0.04	1.13	0.010	0.045	1.132	0.040	1.061	0.040	1.062
6	0.04	0.92	0.020	0.046	0.924	0.042	0.870	0.042	0.871
7	0.05	1.27	0.015	0.058	1.265	0.052	1.202	0.052	1.203
8	0.05	1.03	0.025	0.056	1.033	0.053	0.978	0.053	0.975
9	0.06	1.39	0.015	0.069	1.386	0.065	1.316	0.065	1.316
10	0.06	1.13	0.025	0.068	1.132	0.064	1.107	0.064	1.104
11	0.07	1.50	0.015	0.081	1.497	0.075	1.502	0.075	1.503
12	0.07	1.22	0.025	0.078	1.222	0.078	1.163	0.078	1.161
13	0.08	1.31	0.015	0.087	1.132	0.087	1.295	0.087	1.296

Table 1 includes both the target values and the values measured at the wave gauge array placed in front of the wave maker (see Fig. 3). It is worthy to note that the values of the measured wave height include wave reflection inside the basin, that is why the generated wave heights are up to the 10% greater than the target wave height. For each configuration (6 in total), the wave attacks were repeated by imposing the same wave series and wave energy spectrum generated at the wavemaker with the first configuration

Prior to the hydrodynamic tests, free oscillating tests were performed in absence of incident waves, by applying an instantaneous displacement along each direction, keeping the system in place for a few seconds and then releasing it. During this procedure, the displacements were continuously recorded by the MTi. Surge and yaw modes are usually related to mooring dynamics, whereas pitch and heave are mainly driven by the geometry and by the PTO loads. From these tests on the SeAbacus without PTO, it was found the natural period for pitch around 1.1 s. Therefore, to optimise the power production, the device should operate in a wave climate characterised by a wave period of about 1.1 s

in 1:25 scale, a condition that represents short and steep waves.

3. The device power production capacity

This Section presents the main results in terms of statistical values of the pitch (p) of the oscillating element; specifically, for each test performed, reference is given to the average of the 1/3 ($p_{1/3}$) and of the 1/150 ($p_{1/150}$) of the upper p-values. These statistical values were selected to represent ordinary and extreme conditions. Since the power production is usually assessed in ordinary wave conditions, to avoid oversizing the PTO system, specific focus is on the values of $p_{1/3}$. All the figures are reported for completeness in the Appendix A (Figs. A.1–A.3). In particular, the effects of the shape of the rotating element, of the mooring system type and of the wave obliquity on the pitch are analysed in Sections 3.1, 3.2 and 3.3 respectively. Some comments about the potential device producibility are finally drawn in Section 3.4.

3.1. The effects of the shape

The first analysis carried out focused on the investigation of the role of the shape of the device, to individuate the most promising configuration in terms of power production and concentrate on it for further analyses.

Fig. 5 shows the values of $p_{1/3}$ in both cases of the DD and SD shape – represented respectively with circles and diamonds – moored with the TLP. The corresponding figure for $p_{1/150}$ is reported in Appendix A, Fig. A.1. For both shapes, $p_{1/3}$ increases with increasing H_{si}, following an almost linear trend for H_{si} <0.05 m and apparently reaching a floor for H_{si} >0.05 m.

The DD shape gives systematically lower values of $p_{1/3}$ than the SD shape: for the same H_{si}, the ratio between the values of $p_{1/3}$ obtained with the DD shape ($p_{1/3,DD}$) and the ones obtained with the SD shape ($p_{1/3,SD}$) is almost constant and ≈ 2 for all the tests performed. Evidently, instead of improving the oscillation magnitude thanks to the double Salter's Duck as it was expected to better follow the wave shape both in the crest and in the trough phase, the DD shape results in greater inertia and resistance to flow, and therefore in slower and lower amplitude oscillations. The maximum measured value of $p_{1/3}$ is slightly less than 25° for the SD shape and around 12° for the DD shape.

From Fig. 5, it can be also appreciated that the effect of the wave steepness (sop) plays a more relevant role with the SD than with the DD shape, showing a very sensitive response of the SD oscillating element to rather moderate wave steepness (blue markers) and therefore suggesting that slightly steeper wave attacks (i.e. the steeper case for the same target H_s in Table 1, red markers) as common in other areas of the Mediterranean Sea, would lead to much higher pitches and device producibility.

3.2. The effects of the moorings

Once verified that the SD shape determines higher pitch values and therefore should guarantee higher production rates, the DD configuration was dismissed and further investigations were carried for SD exclusively.

Fig. 6 compares the values of $p_{1/3}$ of the SD in case of TLP, calm and spread mooring systems. The different symbols correspond to the different moorings while the different colours correspond to the cases with the lower and the higher wave steepness given the same target wave height. The corresponding results for $p_{1/150}$ are reported in Fig. A2.

As already observed for the TLP (see Fig. 5 and Section 3.1), for all the moorings the pitch values increase with increasing wave height (till H_{si}≤0.05 m) and then (for H_{si}>0.05 m) tend to an almost constant value. There is a clear effect of the wave steepness, resulting in higher values of $p_{1/3}$ for all the mooring types. For all the different type of moorings, the values of $p_{1/3}$ tend to 15° and 20°, for lower and higher wave steepness respectively.

The TLP mooring performs better (i.e. gives a greater pitch for the same target H_s) for the lower wave steepness and contemporarily for the higher waves (H_s>0.05 m), while the spread mooring performs always slightly better than the calm mooring, especially for higher waves (H_s>0.05 m).

By comparing the results for the same value of H_s, the average difference of $p_{1/3}$ from a TLP to a spread and from a TLP to a calm is respectively -0.53° and +0.83°, with the corresponding standard deviations of +2.71° and +2.82°. The difference of $p_{1/3}$ between a spread and a calm mooring is always positive, being the average difference +1.35°, with a standard deviation of 2.13°. It can be therefore concluded that overall, both the TLP and the spread mooring perform better than the calm mooring. It can be also concluded that the TLP mooring has a

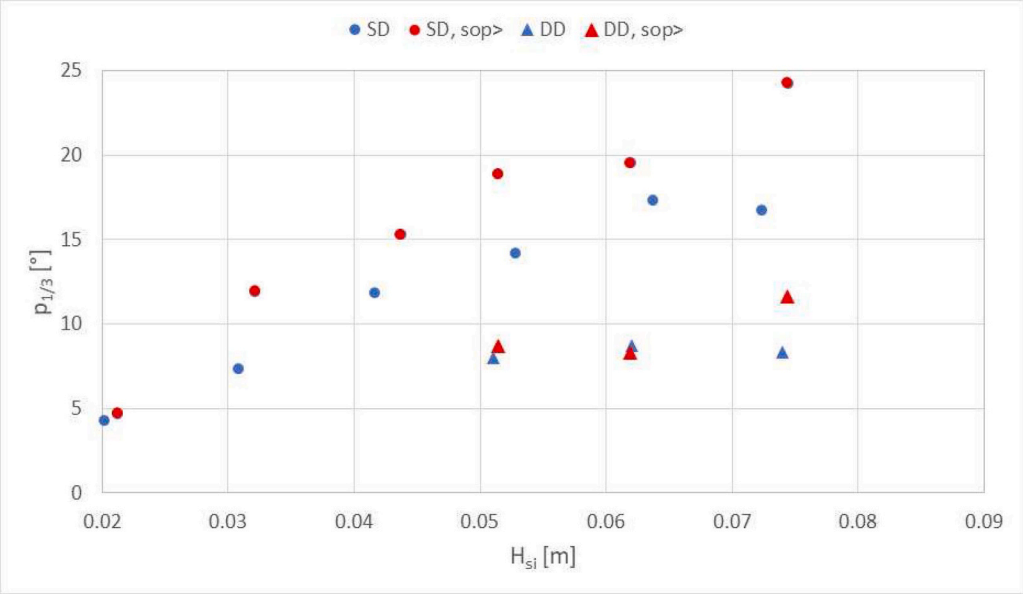

Fig. 5. Pitch ($p_{1/3}$) as a function of the incident wave height for both SD and DD configurations moored with TLP. The steeper case for the same target H_s is denoted by red markers and by the indication "sop>" in the legend.

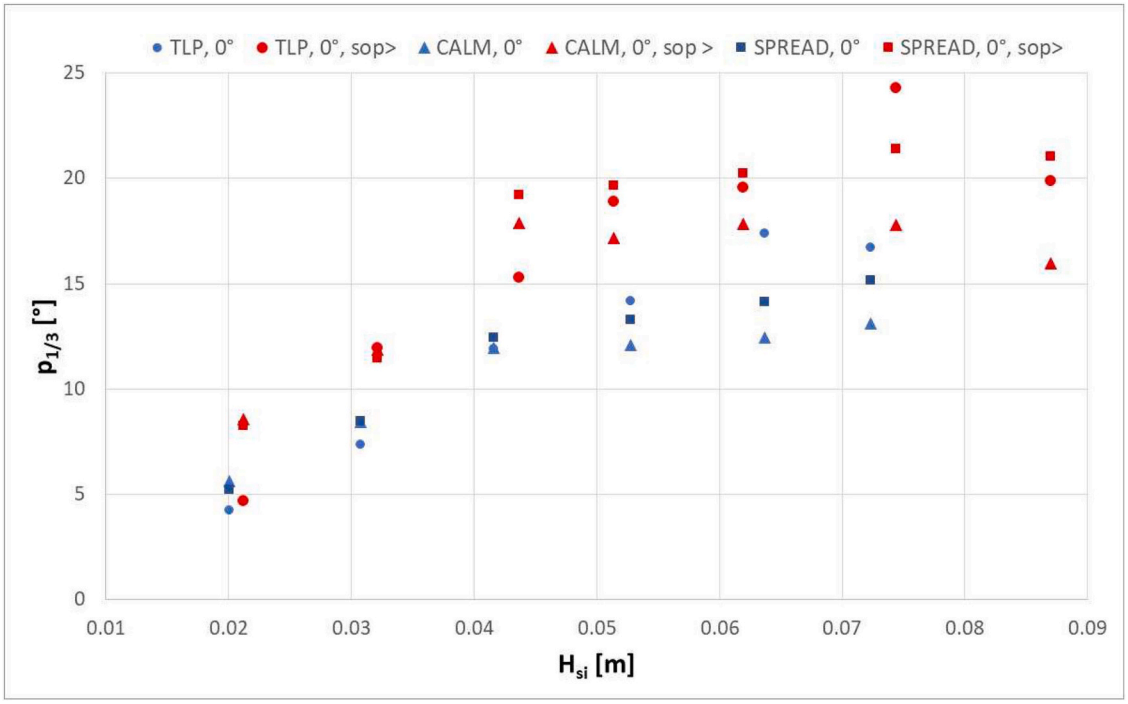

Fig. 6. Pitch values $p_{1/3}$ as a function of the incident wave height for TLP, CALM and SPREAD moorings that are represented by the circles, the triangles and the squares respectively. The red colour identifies the tests characterised by greater wave steepness for the same target wave height. The steeper case for the same target H_s is denoted by red markers and by the indication "sop>" in the legend.

slightly greater performance than the spread in terms of potential producibility. However, the preference is given to the spread mooring that may allow for limited orientation of the device with the waves and that usually results in lower forces on the moorings (to be assessed in the next Section). Moreover, given that the same type of material was adopted for the mooring lines, the TLP mooring has lower cost as for the length of the mooring lines but had greater cost for the complexity of the installation than the spread mooring.

These results, where the better-performance-order list shows first the TLP then the spread and finally the calm, can be justified by the specific construction of the device, where the motion of the raft was not completely disconnected by the motion of the oscillating element. Therefore, the stiffer the mooring, the more rigid is the raft, the greater is the pitch.

3.3. *The effects of the wave obliquity*

The effects of the wave obliquity were investigated by rotating the

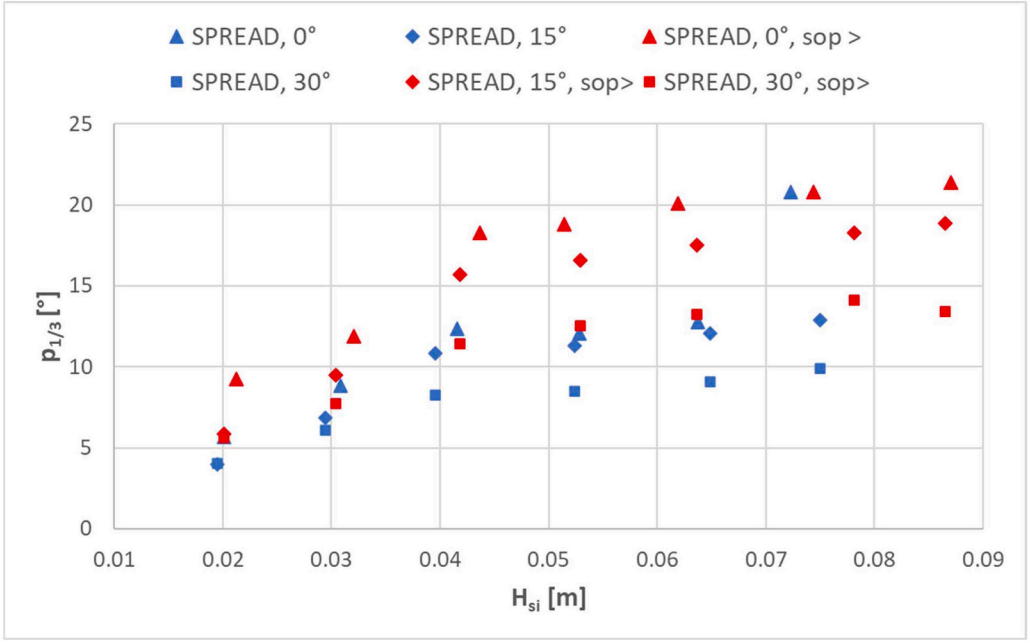

Fig. 7. Pitch values ($p_{1/3}$) as a function of the incident wave height for the spread mooring system and different wave obliquity. The steeper case for the same target H_s is denoted by red markers and by the indication "sop>" in the legend.

device axis in the wave tank by moving the anchors and keeping constant their mutual distance. Two configurations were analysed with the SeAbacus moored with a spread mooring and rotated of 15° and of 30° with respect to the perpendicular to the wave maker. The SPREAD configuration was selected following the outcomes of the sensitivity analysis to the effects of the different mooring configurations presented in Section 3.2. Fig. 7 compares the statistical values of $p_{1/3}$ in case the device axis is perpendicular to the wave basin cross-shore axis (0°) and oriented at 15° and 30° with respect to the wave basin cross-shore axis. The different symbols correspond to the different obliquity while the different colours correspond to the cases with lower and higher wave steepness for the same target wave height.

The pitch values $p_{1/3}$ increase with increasing H_{si} and are strongly affected by the wave obliquity. With increasing H_{si}, the values of $p_{1/3}$ decrease from 18° to 16° and 11° respectively for wave obliquity equal to 0°, 15° and 30°. It can be appreciated that this effect is more evident for the greater tested wave steepness given the same incident wave height.

The effect of the wave steepness is not negligible for each of the tested wave obliquity, given an average reduction of $p_{1/3}$ of the 10% and of the 30% respectively when H_s is lower or higher than 0.04 m. The lower steepness values of $p_{1/3}$ at 15° and the higher steepness values of $p_{1/3}$ at 30° are very close to the lower steepness values of $p_{1/3}$ at 0°.

It can be concluded that the device performance significantly decreases with increasing wave obliquity. These results suggest that more devices can be usefully placed in modules where each device cover a different incoming wave orientation, especially in a wave climate characterised by more than one main direction such as in the Northern Adriatic Sea, where the wave frequencies from North-East and South-East are similar.

3.4. Potential device producibility

The results presented in the previous sub-sections showed that the values of the pitch are strongly affected by the wave steepness, by the mooring type and by the wave obliquity. The pitch of the oscillating element is directly related to the device producibility, since the oscillation with respect to the fixed shaft is the motion generating the electromagnetic field in the selected PTO for future installation.

The maximum values of $p_{1/3}$ of $p_{1/150}$ reach 20° and 37° for the SPREAD, 18° and 22° for the TLP and 13° and 31° for the CALM under perpendicular wave attacks, see Figs. 6 and A.2. By keeping as reference value the maximum value of $p_{1/3}$ obtained with the SPREAD, it can be concluded that the device producibility roughly decreases to the 82% and to the 59% respectively with TLP and CALM in ordinary wave conditions. By repeating a similar consideration for the SPREAD under oblique waves, one derives that the producibility roughly decreases to the 89% and to the 61% respectively at 15° and at 30° with reference to the case of perpendicular waves.

It is worthy to note however that the absence of the PTO with its associated damping and stiffness significantly affects the hydrodynamic response of a WEC and the mooring loads (Elhanafi et al., 2017; Xu et al., 2022). Wave basin tests usually consist of a first phase when the device performance is tested under regular waves, to optimize the PTO rigidity and then of a second phase when the device performance is tested under irregular waves limitedly to the optimal PTO rigidity (Zanuttigh et al., 2013). In this case the absence of the PTO for sure affects the pitch values and therefore the potential power absorption.

These results suggest the need for further research to optimize the shape of the raft, that was kept very simple to reduce construction costs, and to reduce the inertia and optimize the shape of the oscillating element, to increase the oscillation amplitude. Based on the results of these preliminary tests, an upgraded version of this device is under analysis and will be constructed by the end of this year. The new device will include a modified raft and a realistic PTO system to derive direct measurements of the power production.

4. The forces on the mooring lines

This Section presents the main results in terms of statistical values of the Forces on the mooring lines; specifically, reference is given to the average of the 1/3 ($F_{1/3}$) and of the 1/150 ($F_{1/150}$) of the upper values. These statistical values were selected to represent ordinary and extreme conditions. The values of the forces correspond to the values of the most solicited mooring line at the front of the device (off-shore side), for a cautious assessment. Since the device survivability is usually assessed in extreme wave conditions, to verify snapping loads on the moorings, specific focus is on the values of $F_{1/150}$. All the figures are reported for completeness in the Appendix A (Figs. A.4 and A.5). In Section 4.1 the results of the forces for the different mooring systems are compared, while in Section 4.2 the effects of wave obliquity on the mooring forces are analysed for the spread layout.

4.1. Comparison of the forces for mooring type

The results of the forces $F_{1/150}$ (in Fig. 8) show the expected trend of increasing F with increasing H_{si} in case of the SPREAD and CALM moorings. For the TLP instead the forces $F_{1/150}$ show a great scatter with an almost constant trendThe values of $F_{1/3}$ can be found instead in Fig. A.4.

As expected, the forces decrease with decreasing the mooring layout rigidity, i.e. from TLP to SPREAD (of about 6 times) and then from SPREAD to CALM (of about one order of magnitude). The mean and standard deviation values are 58.8 N and 6.2 N for TLP, 12.7 N and 3.8 N for SPREAD and 3.2 N and 2.3 N for CALM respectively.

The results show also a very limited effect of the wave steepness, with overall slight lower values in case of the higher wave steepness for the same target wave height. The greater values of the pitch should be therefore justified by the shape of the oscillating element affecting the relation between its oscillation and the steepness of incoming waves.

4.2. Effects of wave obliquity on the mooring forces for the spread layout

For the spread mooring layout, the results of $F_{1/150}$ are reported for the three tested obliquities (0°, 15°, 30°) as a function of H_{si} in Fig. 9. The values of $F_{1/3}$ can be found instead in Fig. A.5. For all the obliquities, the values of $F_{1/150}$ show always an increasing trend with H_{si} and tend to an almost constant value for $H_{si}>0.07$ m (around 11.8 N, 9.8 N and 7.8 N respectively at 0°, 15° and 30°).

As well as for the pitch values, the values of the forces do not show any significant dependence on the wave steepness at 15° and 30°.

4.3. Spectral analysis

Spectral analysis of the pitch and of the most excited mooring line was carried out for the SPREAD under perpendicular wave attacks. For this system, the spectra are very “clean” both for the pitch and for the force, showing essentially no excited harmonics besides the prominent peaks close to 1, and both the spectra have similar characteristics for all the wave heights, differently from the complex wave attenuator tested by Stansby et al. (2022). Fig. 10 shows two example of the pitch and of the force spectra as a function of the frequency.

Fig. 11 reports the values of the peak frequencies of the pitch and of the force spectra for all the wave attacks. It can be appreciated that the peak frequencies of the pitch spectra are rather constant, varying very limitedly (and randomly) in the range 1.08-1.17 s. This suggests that a period around 1.1 corresponds to the pitch resonance.

The peak frequencies of the force spectra basically follow the trend of the significant frequencies of the wave spectra. The values of the peak frequencies of the force spectra are close and always lower than the values of the significant frequencies of the wave spectra, with the exception of the wave states 2 and 6, where the significant wave frequencies are greater than the peak frequencies of the pitch and of the

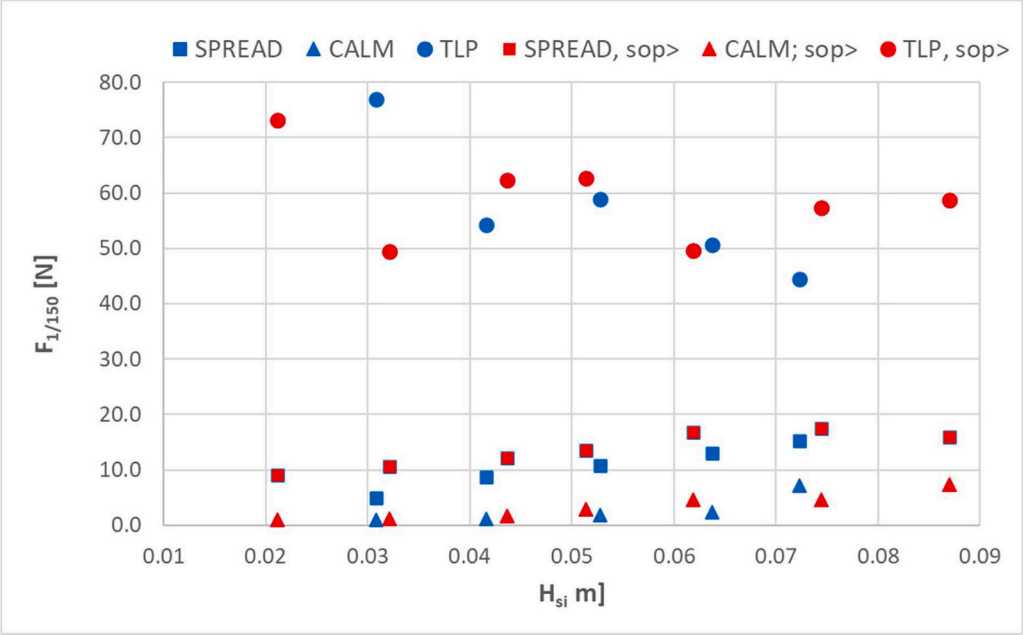

Fig. 8. Forces $F_{1/150}$ as a function of the incident wave height for the three different mooring configurations: TLP, SPREAD and CALM. The steeper case for the same target H_s is denoted by red markers and by the indication "sop>" in the legend.

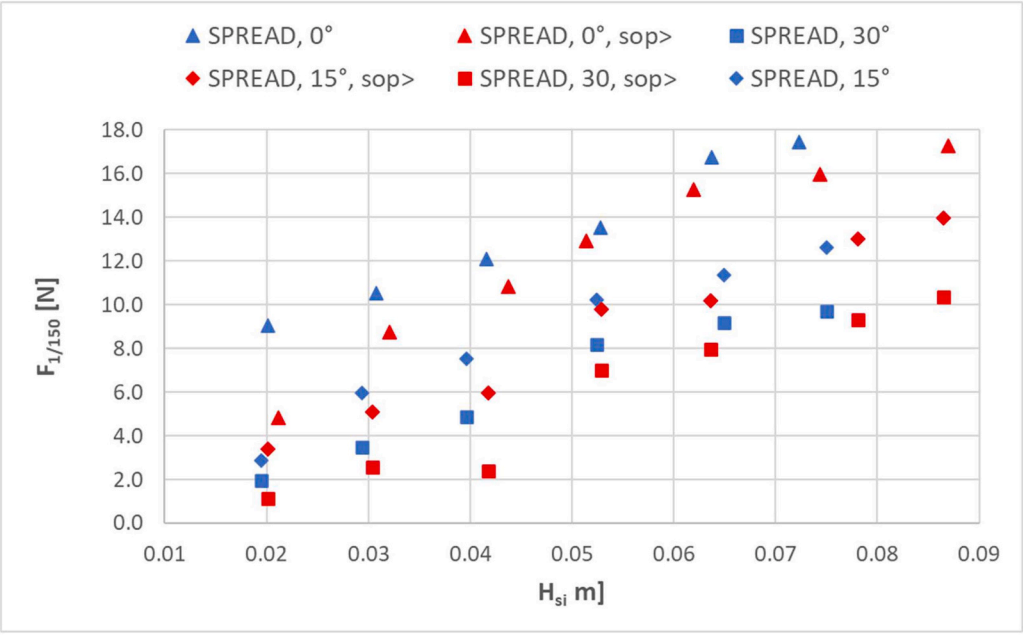

Fig. 9. Values of the forces ($F_{1/150}$) as a function of the incident wave height for the spread mooring system and different wave obliquity. The steeper case for the same target H_s is denoted by red markers and by the indication "sop>" in the legend.

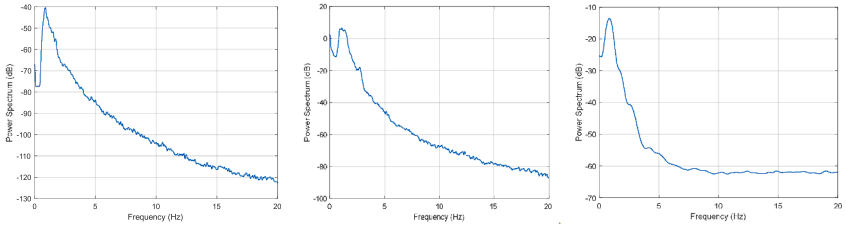

Fig. 10. Sample spectra for wave, pitch, and force, from left to right. Test 10, SPREAD, perpendicular wave attack.

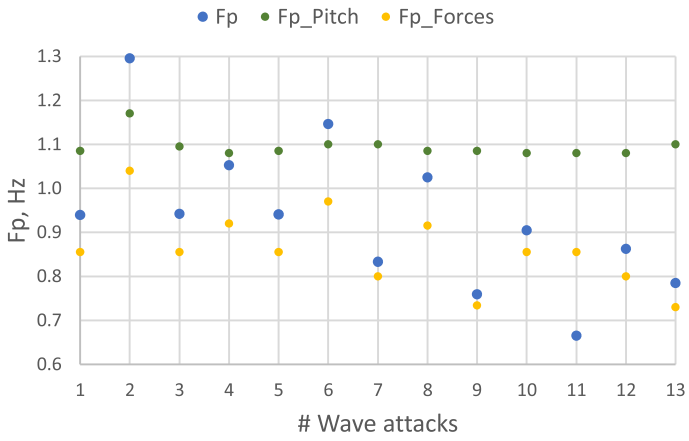

Fig. 11. Values of the pitch peak frequencies and of the forces peak frequencies obtained from spectral analysis for each tested wave state. The significant wave frequency of each incident wave state is also reported.

wave state 11, where the significant wave frequency is the lowest and therefore lower even than the peak frequency of the force. Overall, the peak spectral frequencies of the forces demonstrate that the mooring lines are mostly excited in correspondence of the significant spectral frequencies of the waves, with a short time delay due to the wave impact on the mooring lines and to the inertia of the device motion and of the corresponding mooring system tensioning.

The values of the peak frequencies of the force spectra are always significantly lower than the values of the pitch spectral peak frequencies and the range of the values for the forces is slightly wider than for the pitches, being 0.73-1.04 s.

5. Conclusions

The novel floating wave attenuator SeAbacus was tested in the wave tank at the University of Bologna. The device essentially consists of a rafted Salter's Duck that is expected to produce wave energy based on the pitch amplitude of the Salter's Duck with the waves. Tests were performed with different shapes of the Salter's Duck and different moorings, with varying wave heights, wave steepness and wave obliquity.

The shape of the oscillating element – single or double Salter's Duck – was tested first and clearly proved the single Salter's Duck to provide the user with a significantly greater oscillation amplitude than the double Salter's Duck.

The Salter's Duck pitch motion is significantly affected by the wave steepness and by the wave obliquity. Specifically, the pitch motion increases of about the 30% for the greater tested wave steepness (0.02-0.03 instead of 0.01-0.02) for the same incident wave height. It decreases of about the 10% and the 30% at 15° and 30° respectively if compared with the perpendicular wave attack (10°). These results suggest that the pitch is greater for steeper seas ($\geq$0.025) such as the Tyrrhenian and the Ionian Sea, by limiting the search to the same country and to the same basin only. They suggest also a greater production capability of the device if placed in arrays, with the devices eventually oriented along different directions.

Different moorings were also tested, showing that for this device the best compromise between device pitch motion and mooring load is the spread mooring. The trend of the forces is increasing with the incident wave height and does not show any significant effect of the wave steepness. Under oblique waves, the forces on the moorings decrease on average of about the 75% and the 58% of the values at 0° in case of 15° and 30° respectively. In most cases, the peak frequencies of the force spectra are closely related to the peak frequencies of the wave spectra.

Based on the results of these tests, an upgraded design of the device including a PTO system was developed. The new design was focused on the raft shape and on the Salter's Duck shape to minimise the device inertia while keeping the device stability and to increase the Salter's Duck pitch response to waves. The presence of the PTO system will also allow a direct measurement of the device production and of its damping effect, thanks to the contemporary measurement of the loads on the moorings.

CRediT authorship contribution statement

Barbara Zanuttigh: Writing – review & editing, Writing – original draft, Validation, Methodology, Investigation, Formal analysis, Data curation. **Paola Pareschi:** Investigation, Methodology, Data curation. **Elisa Dallavalle:** Writing – review & editing, Methodology. **Sara Mizar Formentin:** Writing – review & editing. **Maria Gabriella Gaeta:** Investigation, Methodology, Data curation.

Declaration of competing interest

The authors declare the following financial interests/personal relationships which may be considered as potential competing interests: Barbara Zanuttigh has patent #102022000002747 - DISPOSITIVO E PROCEDIMENTO PER PRODURRE ENERGIA ELETTRICA DAL MOTO ONDOSO issued to Ministero delle Imprese e del Made in Italy. If there are other authors, they declare that they have no known competing financial interests or personal relationships that could have appeared to influence the work reported in this paper.

Appendix A

For sake of completeness of the data presentation from one side and of paper readability on the other side, this Appendix includes the statistical results obtained for both the pitch and the mooring force that are not reported in the main text.

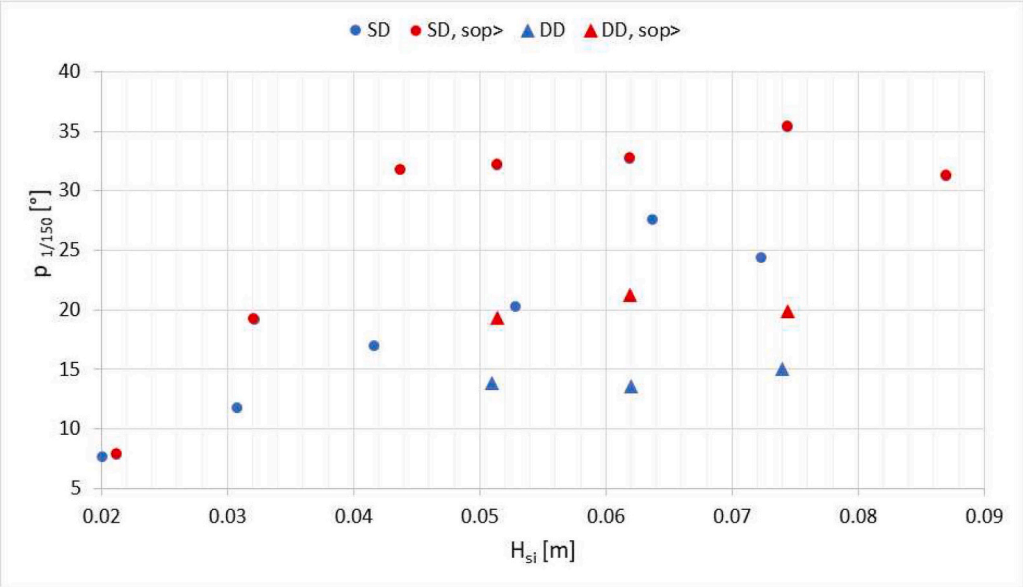

Fig. A.1. Pitch ($p_{1/150}$) as a function of the incident wave height for both SD and DD configurations moored with TLP. The trend is very similar to the one reported in Fig. 5 for the values $p_{1/3}$. The steeper case for the same target H_s is denoted by red markers and by the indication "sop>" in the legend.

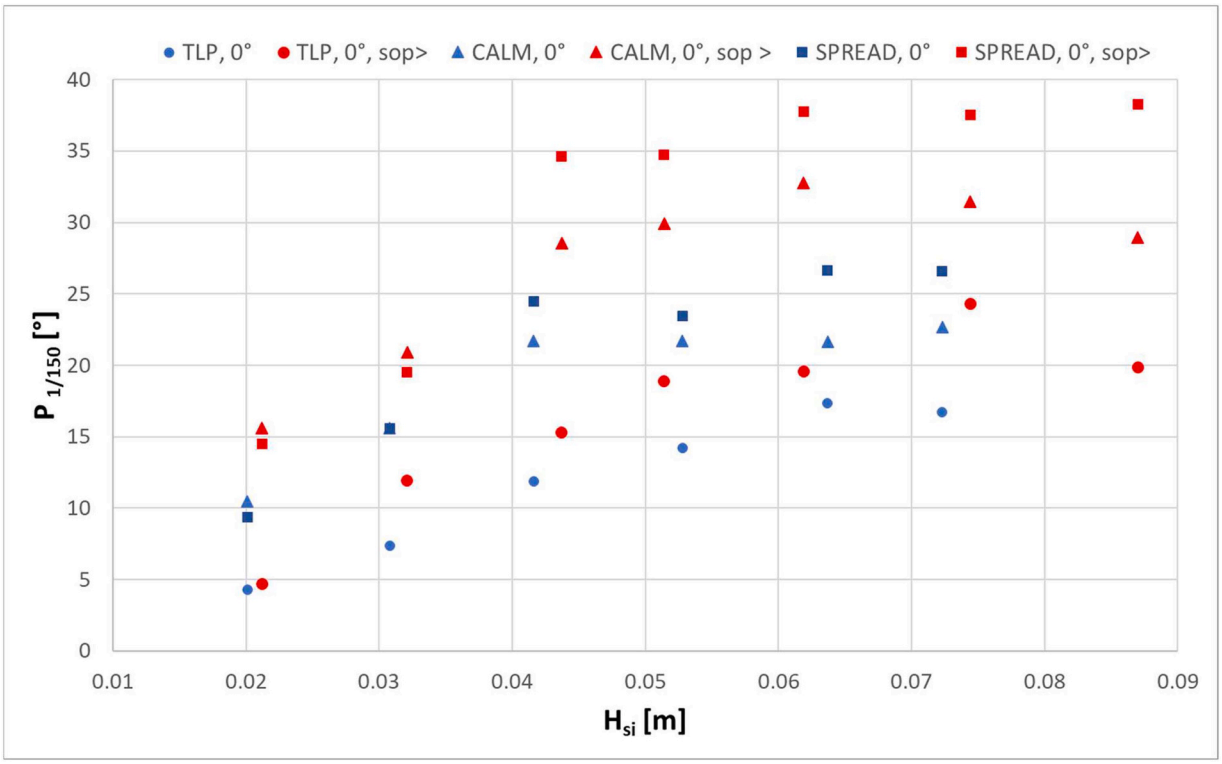

Fig. A.2. Pitch ($p_{1/150}$) as a function of the incident wave height in case of TLP, calm and spread mooring systems. The steeper case for the same target H_s is denoted by red markers and by the indication "sop>" in the legend. For all the moorings the pitch values increase with increasing wave height (till $H_{si} \leq 0.05$ m) and then (for $H_{si} > 0.05$ m) tend to an almost constant value. For all the different type of moorings, the values of $p_{1/3}$ tend to 22° and 30°, for lower and higher wave steepness respectively.

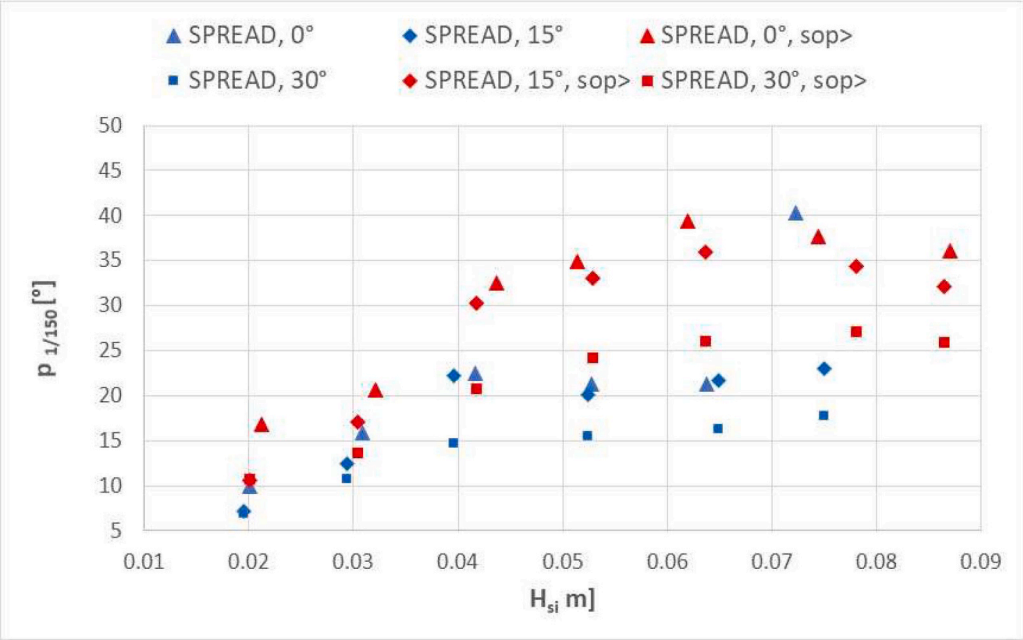

Fig. A.3. Pitch values ($p_{1/150}$) as a function of the incident wave height for the spread mooring system and different wave obliquity. The steeper case for the same target H_s is denoted by red markers and by the indication "sop>" in the legend. The trend of $p_{1/150}$ is very similar to $p_{1/3}$, showing a significant effect of the wave steepness (almost all the upper part of the diagram is characterised by red coloured markers).

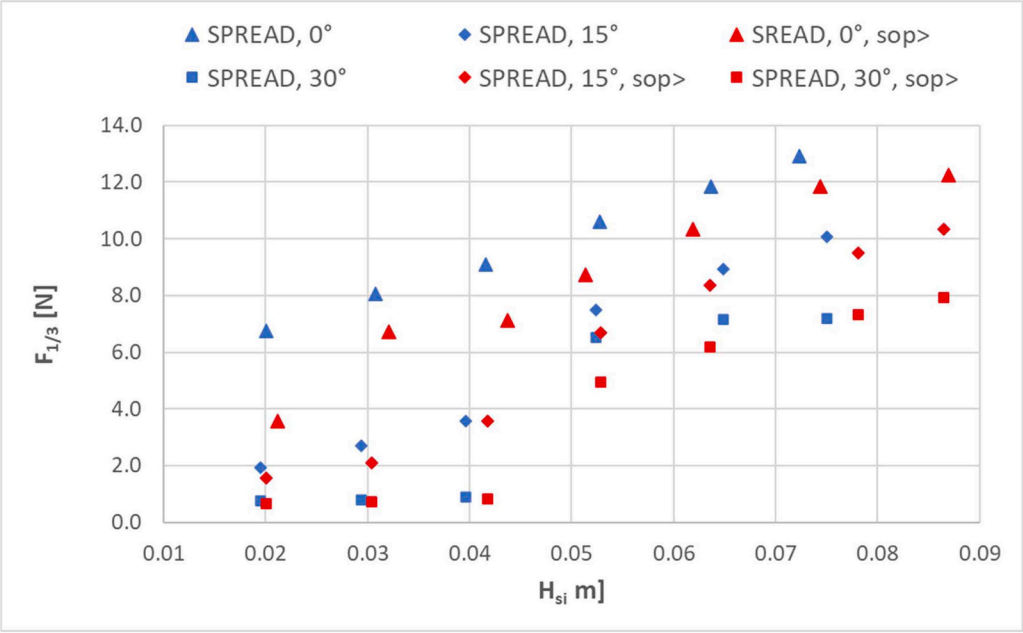

Fig. A.4. Forces $F_{1/3}$ as a function of the incident wave height for the three different mooring configurations: TLP, SPREAD and CALM. The steeper case for the same target H_s is denoted by red markers and by the indication "sop>" in the legend. The forces decrease with decreasing the mooring layout rigidity, i.e. from TLP to SPREAD (of about 1.5 times) and then from SPREAD to CALM (of about one order of magnitude). With increasing Hsi, the values of $F_{1/3}$ tend to 18.6 N, 12.7 N and 1.7 N respectively for TLP, spread and calm moorings.

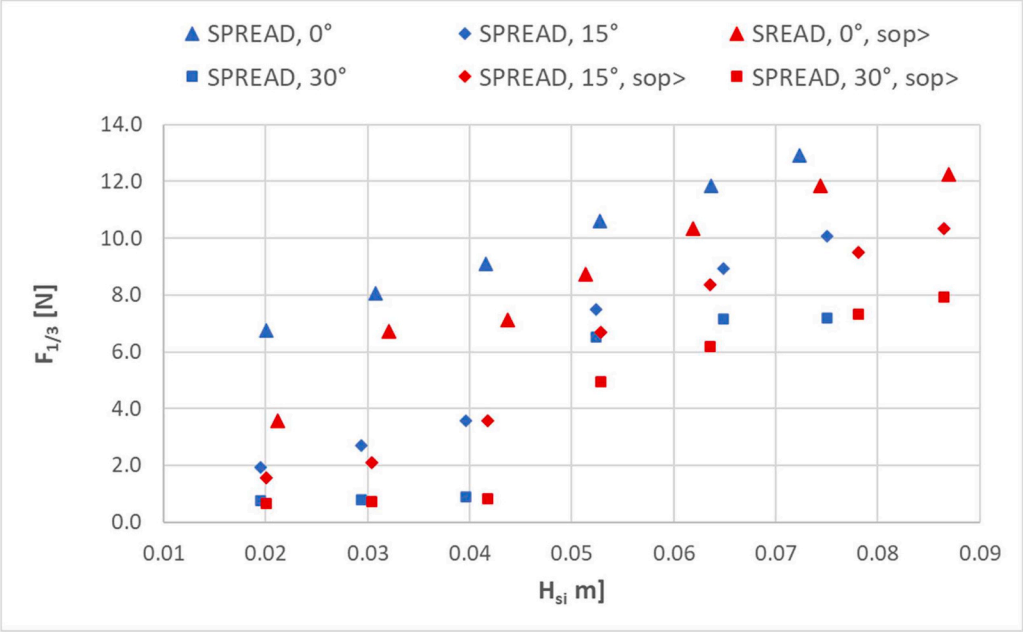

Fig. A.5. Values of the forces $F_{1/3}$ as a function of the incident wave height for the spread mooring system and different wave obliquity. The steeper case for the same target H_s is denoted by red markers and by the indication "sop>" in the legend. The values of the forces significantly decrease with increasing wave obliquity, especially for H_{si} <0.05 m. For H_{si} >0.05 m, the forces increase with H_{si} for all the obliquities, with values on average of about the 75% and the 58% of the values at 0° in case of 15° and 30° respectively. For all the obliquities, the values of $F_{1/3}$ tend to an almost constant value for H_{si}>0.07 m (around 11.8 N, 9.8 N and 7.8 N respectively at 0°, 15° and 30°).

References

Aderinto, T., Li, H., 2018. Ocean wave energy converters: status and challenges. Energies 11 (5), 1250 (Basel).

Arredondo-Galeana, A., Yeter, B., Abad, F., Ordóñez-Sánchez, S., Lotfian, S., Brennan, F., 2023. Material selection framework for lift-based wave energy converters using fuzzy TOPSIS. Energies 16, 7324. https://doi.org/10.3390/en16217324 (Basel).

Bouhrim, H., El Marjani, A., Nechad, R., Hajjout, I., 2024. Ocean wave energy conversion: a review. J. Mar. Sci. Eng. 12 (11), 1922. https://doi.org/10.3390/jmse12111922.

Bruno, M., Maccanti, M., Pulselli, R.M., Sabbetta, A., Neri, E., Patrizi, N., Bastianoni, S., 2022. Benchmarking marine renewable energy technologies through LCA: wave energy converters in the Mediterranean. Front. Energy Res. 10, 980557. https://doi.org/10.3389/fenrg.2022.980557.

Calvário, M., Sutherland, L.S., Guedes Soares, C., 2017. A review of the applications composite materials in wave and tidal energy devices. book: Developments in Maritime Transportation and Harvesting of Sea Resources. In: Proceedings of the 17th International Congress of the International Maritime Association of the Mediterranean (IMAM 2017). Lisbon, Portugal. Publisher: CRC Press. October 9-11, 2017.

Cerveira, F., Fonseca, N., Pascoal, R., 2013. Mooring system influence on the efficiency of wave energy converters. Int. J. Mar. Energy 3–4, 65–81. https://doi.org/10.1016/j.ijome.2013.11.006.

Chatzigiannakou, M.A., Temiz, I.D., 2021. Mooring types of point absorbing wave energy converters. In: Proceedings of the EWTEC 2021. Plymouth, UK. September 2021.

Cruz, J., Salter, S.H., 2006. Numerical and experimental modeling of a modified version of the Edinburgh Duck wave energy device. Proc. Inst. Mech. Eng. M J. Eng. Marit. Environ. 220, 129–147.

Elhanafi, A., Macfarlane, G., Fleming, A., Leong, Z., 2017. Experimental and numerical investigations on the hydrodynamic performance of a floating-moored oscillating water column wave energy converter. Appl. Energy 205, 369–390. https://doi.org/10.1016/j.apenergy.2017.07.138.

Falcão, A., 2010. Wave energy utilization: a review of the technologies. Renew. Sustain. Energy Rev. 14 (3), 899–918.

Foteinis, S., Tsoutos, T., 2017. Strategies to improve sustainability and offset the initial high capital expenditure of wave energy converters (WECs). Renew. Sustain. Energy Rev. 70, 775–785.

Garcia-Teruel, A., Forehand, D.I.M., 2021. A review of geometry optimisation of wave energy converters. Renew. Sustain. Energy Rev. 139, 110593.

Golbaz, D., Asadi, R., Amini, E., Mehdipour, H., Nasiri, M., Etaati, B., Naeeni, S.T.O., Neshat, M., Mirjalili, S., Gandomi, A.H., 2022. Layout and design optimization of ocean wave energy converters: a scoping review of state-of-the-art canonical, hybrid, cooperative, and combinatorial optimization methods. Energy Rep. 8, 15446–15479.

Guo, B., Ringwood, J.V., 2021. A review of wave energy technology from a research and commercial perspective. IET Renew. Power Gener. 15 (14), 3065–3090.

IMAGINE, 2020. https://h2020-imagine.eu/ (accessed October 10, 2025).

Jahangir, M.H., Tayebi, M., Najafabadi, S.G., 2025. A comparative life cycle assessment of three wave energy converters with an economic-environmental approach. Ocean Eng. 329, 121080.

Katalinić, M., Parunov, J., 2018. Wave statistics in the Adriatic Sea based on 24 years of satellite measurements. Ocean Eng. 158, 378–388. https://doi.org/10.1016/j.oceaneng.2018.04.009. ISSN 0029-8018.

Koca, K., Kortenhaus, A., Oumeraci, H., Zanuttigh, B., Angelelli, E., Cantu, M., Suffredini, R., Franceschi, G., 2013. Recent advances in the development of wave energy converters. In: Proceedings of the 10th European Wave and Tidal Energy Conference. Aalborg, Denmark.

Margheritini, L., Kofoed, J.P., 2019. WEPTOS wave energy converters to cover the energy needs of a small island. Energies 12 (3), 423 (Basel).

Martinelli, L., Zanuttigh, B., 2018. Effects of mooring compliancy on the mooring forces, power production, and dynamics of a floating wave activated body energy converter. Energies 11 (12), 3535 (Basel).

Niosi, F., Parrinello, L., Paduano, B., Pasta, E., Carapellese, F., Bracco, G., 2021. On the influence of mooring in wave energy converters productivity: the PeWEC case. In: Proceedings of the International Conference on Electrical, Computer, Communications and Mechatronics Engineering (ICECCME), 7-8 October 2021. Mauritius.

Qiao, D., Haider, R., Yan, J., Ning, D., Li, B., 2020. Review of wave energy converter and design of mooring system. Sustainability 12 (19), 8251.

Romano, A., Bellotti, G., Briganti, R., Franco, L., 2014. Uncertainties in the physical modelling of the wave overtopping over a rubble mound breakwater: the role of the seeding number and of the test duration. Coast. Eng. 103, 15–21.

Stansby, P., Draycott, S., Li, G., Zhao, C., Carpintero Moreno, E., Pillai, A., Johanning, L., 2022. Experimental study of mooring forces on the multi-float WEC M4 in large waves with buoy and elastic cables. Ocean Eng. 266, 113049.

Wu, J., Yao, Y., Li, W., Zhou, L., Göteman, M., 2017. Optimizing the performance of solo duck wave energy converter in tide. Energies 10, 289 (Basel).

Xu, S., Wang, S., Guedes Soares, C., 2019. Review of mooring design for floating wave energy converters. Renew. Sustain. Energy Rev. 111, 595–621.

Xu, S., Wang, S., Guedes Soares, C., 2021. Experimental investigation on the influence of hybrid mooring system configuration and mooring material on the hydrodynamic performance of a point absorber. Ocean Eng. 233, 109178. https://doi.org/10.1016/j.oceaneng.2021.109178. ISSN 0029-8018.

Xu, S., Rezanejad, K., Gadelho, J.F.M., Guedes Soares, C., 2022. Influence of the power take-off damping of a dual chamber floating oscillating water column on the mooring fatigue damage. Ocean Eng. 249, 110832. https://doi.org/10.1016/j.oceaneng.2022.110832. ISSN 0029-8018.

Yazdi, H., Ghafari, H.R., Ghassemi, H., He, G., Karimirad, M., 2023. Wave power extraction by Multi-Salter's duck WECs arrayed on the floating offshore wind turbine platform. Energy 278 (Part A), 27930. https://doi.org/10.1016/j.energy.2023.127930. ISSN 0360-5442.

Zanuttigh, B., Angelelli, E., Kofoed, J.P., 2013. Effects of mooring systems on the performance of a wave activated body energy converter. Renew. Energy 57 (9), 422–431.
Zhao, C., Khalid, F., Lewis, T., Barrett, S., McSwiney, B., Pascal, R.C.R., Kahn, B., Johanning, L., 2025. Advancements in mooring systems for the OE35 wave energy converter: Dynamic design and validation. Ocean Eng. 330, 121235.
Zhang, C., Huang, S., You, Y., Sheng, S., 2019. Numerical research and open sea tests of a 100 kW modified Edinburgh duck wave energy convertor. Front. Energy Res. 7, 120. https://doi.org/10.3389/fenrg.2019.00120.